two Ura$^+$ spores showed a 2:2 segregation for reduced immunological reactivity with the anti-ATPase antibody on Western blots and a reduced intensity of the M_r 100,000 (100K) band representing the ATPase on Coomassie blue-stained gels. The cosegregation of the reduced amounts of the ATPase with the genetic alteration in the *PMA1* gene supports the conclusion that the *PMA1* gene encodes the ATPase. The *Eco*RI subfragment is wholly internal to the *PMA1* gene, therefore its integration leads to disruption of the coding region (Fig. 1*A*). After sporulation and tetrad dissection, the *Eco*RI-transformed diploid gave only two viable spores in each tetrad and the surviving spores were all Ura$^-$. These results show that cells lacking a functional *PMA1* gene are not viable.

The requirement of a functional plasma membrane ATPase for viability could be explained in several ways. One likely possibility is that this H^+ pump is required for active nutrient transport and for *p*H regulation[1]. In addition, the ATPase protein may be required to maintain integrity of the plasma membrane. Such possibilities can now be investigated by further mutational analysis of the cloned gene.

We thank Richard A. Young for the genomic yeast DNA library in λgt11 and the bacterial strains Y1090 and Y1089; David Botstein for the YEp24 library; Mark Rose for the YCp50 library; and Rick Gaber, George Natsoulis and Gary E. Schull for technical advice. We also thank Gary E. Shull and David H. MacLennan for making available the sequences of the animal ATPases before publication. M.C.K.-B. was on leave from the Carlsberg Laboratory, Copenhagen, Denmark and R.S. (on leave from the Instituto de Enzimologia CSIC, Madrid, Spain) was supported by an EMBO fellowship. Antibody preparation was supported by a grant of the CAICYT (Spain) to R.S. This work was supported by NIH grants CM 35010 and CA 34429 to G.R.F., who is an American Cancer Society Research Professor of Genetics.

Received 10 September; accepted 8 November 1985.

1. Serrano, R. *Curr. Topics cell. Regul.* **23,** 87-126 (1984).
2. Young, R. A. & Davis, R. W. in *Genetic Engineering: Principles and Methods* Vol. 7 (eds Setlow, J. K. & Hollaender, A.) 29-41 (Plenum, New York, 1985).
3. Melpartida, F. & Serrano, R. *Eur. J. Biochem.* **116,** 413-417 (1981).
4. Mihara, K. & Blobel, G. *Proc. natn. Acad. Sci. U.S.A.* **77,** 4160-4164 (1980).
5. Drescher, D. G. & Lee, K. S. *Analyt. Biochem.* **84,** 559-569 (1978).
6. Thomas, R. E., Korzeniowski, D., Ryan, D. & Levin, W. *Archs Biochem. Biophys.* **192,** 524-532 (1979).
7. Burnette, W. N. *Analyt. Biochem.* **112,** 195-203 (1981).
8. Rott, R. & Nelson, N. *J. biol. Chem.* **256,** 9224-9228 (1981).
9. Huynh, T. V., Young, R. A. & Davis, R. W. in *DNA Cloning Techniques: A Practical Approach* (ed. Glover, D.) (IRL, Oxford, in the press).
10. Norrander, J., Kempe, T. & Messing, J. *Gene* **26,** 101-106 (1983).
11. Pikielny, G. W., Teem, J. L. & Rosbash, M. *Cell* **34,** 395-403 (1983).
12. Hesse, J. E. *et al. Proc. natn. Acad. Sci. U.S.A.* **81,** 4746-4750 (1984).
13. Shull, G. E., Schwartz, A. & Lingrel, J. B. *Nature* **316,** 691-695 (1985).
14. MacLennan, D. H., Brandl, C., Korczak, B. & Green, N. M. *Nature* **316,** 696-700 (1985).
15. Walderhaug, M. O., Post, R. L., Saccomani, G., Leonard, R. T. & Briskin, D. P. *J. biol. Chem.* **260,** 3852-3859 (1985).
16. Farley, R. A. & Faller, L. D. *J. biol. Chem.* **260,** 3899-3901 (1985).
17. Dame, J. B. & Scarborough, G. A. *J. biol. Chem.* **256,** 10727-10730 (1981).
18. Berry, E. A. & Hinkle, P. C. *J. biol. Chem.* **258,** 1474-1486 (1983).
19. Ovchinnikov, Y. A., Abdulaev, N. G. & Modyanov, N. N. *A. Rev. Biophys. Bioengng* **11,** 445-463 (1982).
20. Schwartz, D. C. & Cantor, C. R. *Cell* **37,** 67-75 (1984).
21. Carle, G. F. & Olson, M. V. *Nucleic Acids Res.* **12,** 5647-5664 (1984).
22. Hsu, Y. P. & Schimmel, P. *J. biol. Chem.* **259,** 3714-3719 (1984).
23. Downie, J. A., Gibson, F. & Cox, G. B. *A. Rev. Biochem.* **48,** 103-131 (1979).
24. Orr-Weaver, T. L., Szostak, J. W. & Rothstein, R. J. *Proc. natn. Acad. Sci. U.S.A.* **78,** 6354-6358 (1981).
25. Maxam, A. M. & Gilbert, W. *Meth. Enzym.* **65,** 499-560 (1980).
26. Bencini, D. A., O'Donovan, G. A. & Wild, J. R. *Biotechniques* **2,** 1-70 (1984).
27. Heffron, F., So, M. & McCarthy, B. J. *Proc. natn. Acad. Sci. U.S.A.* **75,** 6012-6016 (1978).
28. Staden, R. *Nucleic Acids Res.* **10,** 2951-2961 (1982).
29. Kyte, J. & Doolittle, R. F. *J. molec. Biol.* **157,** 105-132 (1982).
30. Eisenberg, D. *A. Rev. Biochem.* **53,** 595-623 (1984).
31. Serrano, R. *FEBS Lett.* **156,** 11-14 (1983).

Location of exit channel for nascent protein in 80S ribosome

R. A. Milligan & P. N. T. Unwin

Department of Cell Biology, Stanford University School of Medicine, Stanford, California 94305, USA

Ribosomes crystallize on endoplasmic reticulum membranes in oocytes of the southern Italian lizard, *Lacerta sicula*, during winter[1]. Electron crystallographic studies of the crystals have been made to elucidate the arrangement of the ribosomal subunits on the membrane surface[2,3]. We have now obtained more extensive and better ordered crystals of the same habit, grown from chick embryo ribosomes[4], and report here on their native structure preserved by rapid freezing of the crystals in thin aqueous films. The three-dimensional map reveals new details of the protein and ribosomal RNA distribution within the ribosome. Most striking is a region of low density within the large subunit which extends from the subunit interface towards an area on the membrane-facing surface identified by others[5,6] as the exit site of the nascent protein. This region of low density appears to delineate the path taken by the growing polypeptide through the ribosome to the external surface.

The chick embryo crystals (Fig. 1) are composed of ribosome tetramers in two opposite-facing layers, arranged in the two-sided plane group $p42_12$ ($a = 593$ Å). Each of the layers, when viewed from the mid-plane of the crystal, presents a right-handed p4 lattice, which identifies their outermost surfaces as being equivalent to the surface which, in the lizard, attaches to the membrane[3]. Specimens were prepared for electron microscopy by rapid freezing in thin aqueous films[7,8], and images were recorded of the specimens tilted at angles of up to 50° with respect to the incident electron beam. The images were analysed by standard methods[9] to provide a three-dimensional dataset of

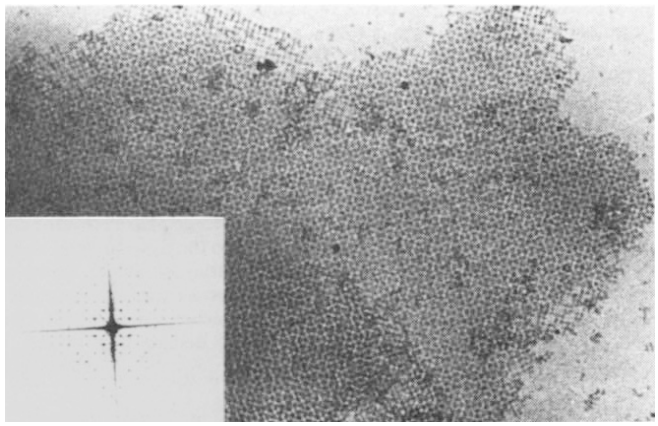

Fig. 1 Image of a ribosome crystal (×37,500) embedded in a thin film of frozen buffer, and optical diffraction pattern (inset) from an area containing ~15×15 unit cells. The crystal was tilted at an angle of 10° to the incident electron beam.

Methods. Crystals, prepared as described in ref. 4, were washed free of mother liquor by low-speed centrifugation and resuspended in a solution in which ribosomes are potentially active (50 mM KCl, 10 mM $MgCl_2$, 0.5 mM EDTA, 0.5 mM dithiothreitol, 10 mM HEPES *p*H 7.2). They were applied in 5-μl aliquots to amylamine-treated carbon-coated grids and, after the excess liquid had been blotted off, were quick-frozen by plunging the grids into liquid ethane slush[7,8]. The grids were mounted under liquid nitrogen in a Philips cold holder, PW 6591/00, and examined at −160 °C using an EM400 electron microscope operating at 100 kV. Protection of the grid by an additional anti-contamination device[21] was necessary during the 10 min after insertion. Only one image was recorded from each frozen crystal. Each area photographed received a total dose of 2-5 electrons per Å^2. Images were recorded at an electron optical magnification of ×19,500 or ×15,200 with an underfocus (2.0-2.5 μm) such that the first zero of the contrast transfer function lay just outside the resolution (1/55 Å^{-1}) to which the diffraction patterns extended.

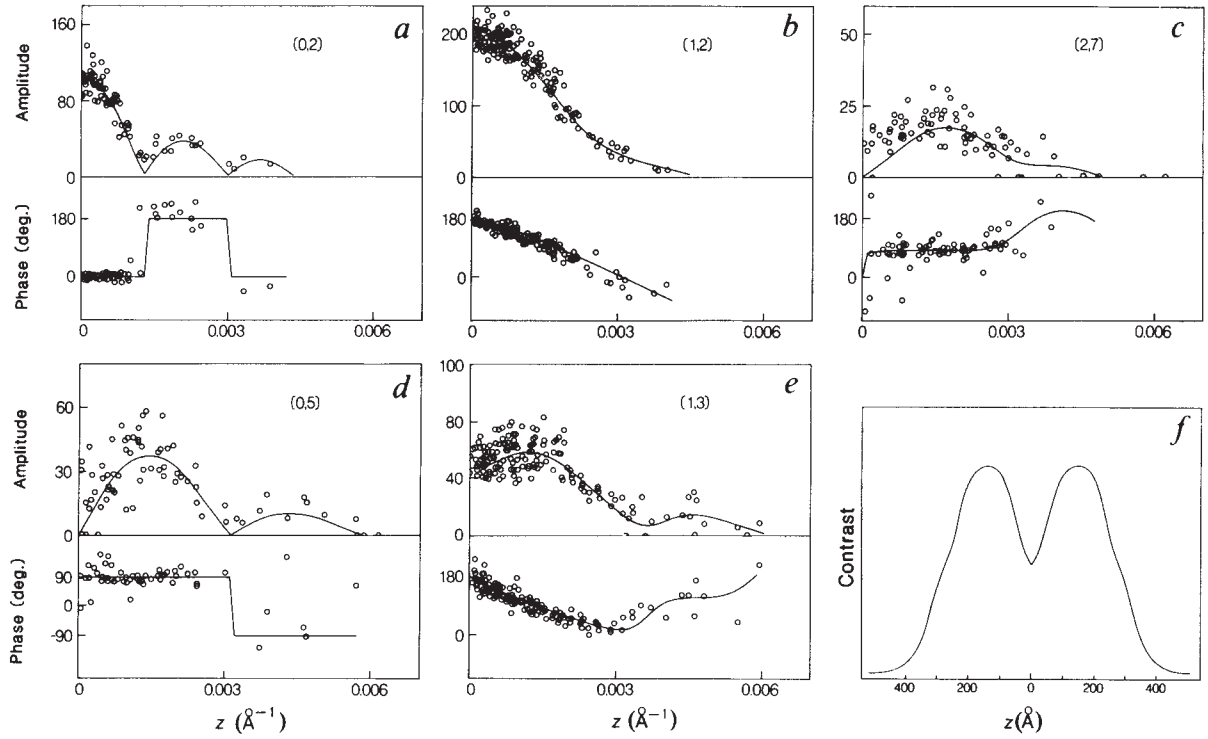

Fig. 2 *a–e*, Variations of amplitude and phase along 5 of the 42 lattice lines from which the three-dimensional map was synthesized ($p42_12$ symmetry imposed). Open circles represent the experimental values obtained by computer processing of the images, solid lines the fitted curves. z^*, is the distance from the mid-point of the lattice line. *f*, Plots of the contrast (maximum density minus minimum density in each section) through the map in the direction perpendicular to the plane of the crystal. The crests of the peaks which represent the two ribosome layers are separated by ~280 Å.

Methods. Computer processing of images was done in the standard way[9]. Highly ordered areas in the images were selected by optical diffraction and scanned with a Perkin-Elmer microdensitometer having step and sampling sizes of 25 μm, corresponding to 13 Å at the specimen. We calculated Fourier transforms (512 × 512) of the optical density arrays thus generated, and reciprocal lattices were fitted to the strong peaks. Amplitudes and phases of above-background peaks were extracted at the reciprocal lattice points to the resolution observed in the optical diffraction patterns. Several images of untilted crystals giving average phase residuals of <25°, based on a comparison of individual 4-fold related peaks, were used for the initial data in the three-dimensional analysis. Thirty-nine images from tilted crystals (tilt angle range 4–50°) were used for the remaining data, the tilt axis and angle parameters being calculated from the distortion of the reciprocal lattice. The data were first combined assuming p4 symmetry, using a comparison range in z^* of 0.001 $Å^{-1}$. After we had ascertained that the ribosomes in the two crystal layers were equally well preserved—that is, showing the same essential features independent of the layer in question—the data were combined with $p42_12$ symmetry. The average phase error for each image, based on a cumulative comparison of individual symmetry-related phases, was 22°. Smooth curves were fitted to the experimental values along each lattice line[22] and the curves were sampled at regular intervals (1/1,500 $Å^{-1}$) to provide the terms for Fourier synthesis. Terms along the 0,0 lattice line were not included. No corrections were made to compensate for the effects of the phase-contrast transfer function as the background amplitude in the computed transforms showed only a 10–20% change in the range of spatial frequencies over which data were collected. Sections through the map were traced onto plastic sheets which were stacked up to show the overall density distribution. The molecular boundary was chosen to be that at which ribosomes in a tetramer just make contact.

42 crystallographically independent lattice lines, extending to a resolution of ~55 Å (Fig. 2*a–e*). The map was calculated by Fourier synthesis of terms obtained by sampling at regular intervals the continuous variations of amplitude and phase along each of the lattice lines. A plot of the contrast through the structure normal to the plane of the crystal (Fig. 2*f*) shows the separation between the centres of mass of the two layers to be ~280 Å, in good agreement with the 266-Å spacing for this distance measured from low-angle X-ray diffraction patterns[4].

Unlike structures determined from negatively stained specimens, where only stain-accessible surfaces are revealed, the three-dimensional map presented here (Fig. 3) gives a description of the native densities within the ribosome as the crystals have been preserved unstained and frozen in an appropriate ionic environment. Viewed with the membrane-facing surface at the bottom (Fig. 3*a*, *b*), the ribosome forms a rounded outline with two indentations (arrowheads in Fig. 3*a*) suggestive of a partitioning into a larger portion (the large subunit) closest to the 4-fold axis of the tetramer, and a smaller ~210-Å-long portion (the small subunit) at the periphery. Viewed with the membrane-facing surface uppermost (Fig. 3*c*), the ribosome surface comes closest to the observer in a region of the large subunit (M in Fig. 3*c*) identified previously as the salt-sensitive membrane attachment site[2]. Within the ribosome there is a dense core of irregular shape (shading in Fig. 3*b*, *c*), which must be composed largely of rRNA (the most strongly scattering component), because essentially only this density is visualized when contrast from the protein is matched out in a solution containing 10% metrizamide (data not shown). Apparently, much of the interface area between the two subunits is composed of rRNA.

These details are in good agreement with those found in earlier studies. The assignment for the ribosomal subunits corresponds to that determined by comparing maps from arrays of tetramers in negative stain with and without the small subunit present[3]. As before, it appears that the subunits lie approximately side-by-side on the endoplasmic reticulum membrane and are attached to it through a part protruding from the large subunit. Consistent with contrast-matching studies at lower resolution using neutron[10,11] and electron[12] irradiation, the rRNA and protein are distributed inhomogeneously, with rRNA-rich regions concentrated in the interior of the particle.

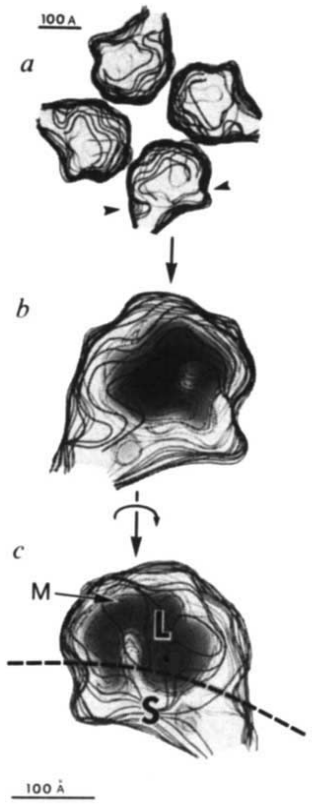

Fig. 3 Three-dimensional contour map showing: *a*, a ribosome tetramer viewed from the mid-plane of the crystal so that the cytoplasmic-facing surface of the ribosome (see text) is closest to the observer; *b*, a single ribosome viewed from the same direction; *c*, a single ribosome viewed so that the membrane-facing surface is closest to the observer. In *a* the molecular boundary alone is shown; contours are incomplete at the periphery, where tetramers in a single layer of the crystal make contact, and at the top (clearer contours) where the two layers of ribosomes in the crystal touch. Arrowheads in *a* and the broken line in *c* follow the surface indentations which appear to identify the boundary between the large (L) and small (S) subunits. The shading in *b* and *c* indicates the distribution of the high-density (rRNA-rich) regions; it makes up 25% of the total volume, or ~65% of the rRNA if one were to assume complete partitioning of the rRNA and protein. M is the part of the large subunit closest to the membrane (see also Fig. 4). Negative stain has been shown to penetrate parts of the structure adjacent to the central region of low density in *c*[2,23].

The feature of particular interest, revealed by this higher resolution analysis, is a narrow elongated region of low density passing through the RNA-rich core at an angle of ~30° to the presumed subunit interface (Fig. 4). This feature does not span the ribosome completely, but appears to originate internally, near the subunit interface, and terminate at a point on the surface of the large subunit close to the membrane attachment site—a total distance of 150–200 Å. Based on correlations made between ribosomes analysed in crystals and isolated ribosomes studied by immunoelectron microscopy[6], the point of intersection with the ribosome surface is close to the exit site of the nascent protein. The low-density region therefore appears to make a direct line between the site at which the growing polypeptide originates, the subunit interface (see refs 13, 14), and the place where the polypeptide emerges from the ribosome. We conclude that the low-density region represents the location of a channel or deep groove in the large subunit along which the growing polypeptide is able to pass.

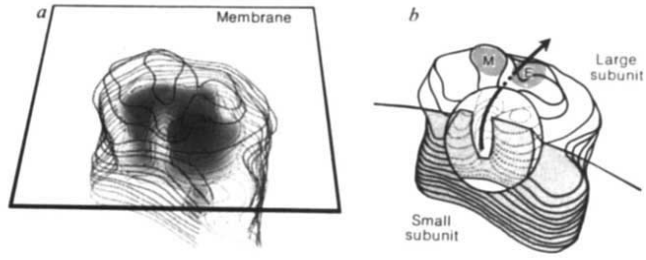

Fig. 4 *a*, Oblique view of the ribosome with the membrane-facing surface towards the observer; *b*, schematic representation of the details revealed. The arrow in *b* indicates the presumed pathway of the polypeptide chain, based on the distribution of low densities in *a*. The point of emergence from the large ribosomal subunit appears to be close to both the membrane attachment site (M)[2] and the exit site (E) determined by immunoelectron microscopy[5,6].

Our results support the deductions made about the location of the channel by Lake and colleagues[6], based on immunolabelling of nascent protein attached to isolated eukaryotic ribosomes. The channel is clearly long enough to account for the observation that up to 39 amino-acid residues are protected from proteolytic enzymes by the large subunit[15–17]. Given that the channel is at least 150 Å long, the enclosed polypeptide is presumably in an extended conformation, implying a bore size of not greater than ~10 Å. A larger diameter would allow formation of secondary structure, so that a much greater portion of the nascent protein than has been found experimentally would be protected. As details of dimensions as small as 10 Å are beyond the resolution of the map, the most likely explanation for the prominence of the low-density path is that the channel is surrounded by ribosomal protein and that the two together make up the observed extensive region of low electron-scattering density. The orientation of the channel seems an ideal one to deliver the polypeptide from the site of translation between the subunits to a point on the external surface adjacent to the membrane where it is optimally located to interact with components of the translocation apparatus such as the signal recognition particle[18], docking protein[19] and the ribophorins[20].

We thank Jacques Dubochet, David Grano and Jean Lepault for their help. This research was made possible by grants and fellowships from the NIH, SERC/NATO, EMBO and the Royal Society.

Received 11 September; accepted 13 December 1985.

1. Taddei, C. *Expl Cell Res.* **70,** 285–292 (1972).
2. Unwin, P. N. T. *Nature* **269,** 118–122 (1977).
3. Unwin, P. N. T. *J. molec. Biol.* **132,** 69–84 (1979).
4. Milligan, R. A. & Unwin, P. N. T. *J. Cell Biol.* **95,** 648–653 (1982).
5. Bernabeu, C. & Lake, J. A. *Proc. natn. Acad. Sci. U.S.A.* **79,** 3111–3115 (1982).
6. Bernabeu, C., Tobin, E. M., Fowler, A., Zabin, I. & Lake, J. A. *J. Cell Biol.* **96,** 1471–1474 (1983).
7. Lepault, J., Booy, F. P. & Dubochet, J. *J. Microsc.* **129,** 89–102 (1983).
8. Milligan, R. A., Brisson, A. & Unwin, P. N. T. *Ultramicroscopy* **13,** 1–10 (1984).
9. Amos, L. A., Henderson, R. & Unwin, P. N. T. *Prog. Biophys. molec. Biol.* **39,** 183–231 (1982).
10. Serdyuk, I. N., Grenader, A. K. & Zaccai, G. *J. molec. Biol.* **135,** 691–707 (1979).
11. Stuhrmann, H. B. *et al. J. molec. Biol.* **119,** 203–212 (1978).
12. Kühlbrandt, W. & Unwin, P. N. T. *J. molec. Biol.* **156,** 431–448 (1982).
13. Liljas, A. *Prog. Biophys. molec. Biol.* **40,** 161–228 (1982).
14. Noller, H. F. *A. Rev. Biochem.* **53,** 119–162 (1984).
15. Malkin, L. I. & Rich, A. *J. molec. Biol.* **26,** 329–346 (1967).
16. Blobel, G. & Sabatini, D. D. *J. Cell Biol.* **45,** 130–145 (1970).
17. Smith, W. P., Tai, P.-C. & Davis, B. D. *Proc. natn. Acad. Sci. U.S.A.* **75,** 5922–5925 (1978).
18. Walter, P. & Blobel, G. *Nature* **299,** 691–698 (1982).
19. Meyer, D. I., Krause, E. & Dobberstein, B. *Nature* **297,** 647–650 (1982).
20. Kreibich, G., Ulrich, B. L. & Sabatini, D. D. *J. Cell Biol.* **77,** 464–487 (1978).
21. Homo, J.-C., Booy, F., Labouesse, P., Lepault, J. & Dubochet, J. *J. Microsc.* **136,** 337–340 (1984).
22. Agard, D. A. *J. molec. Biol.* **167,** 849–852 (1983).
23. Milligan, R. A. thesis, Stanford Univ. (1985).